An IGFBM-SAA Fast Algorithm for Solving Electromagnetic Scattering from Layered Media Rough Surfaces

Lilan Lei

School of Mathematics and Computer Science
Yichun University, Yichun 336000, China
lilanlei0320@126.com

Abstract – This article proposes a new fast solution algorithm (IGFBM-SAA), which combines the Improved Generalized Forward and Backward Method (IGFBM) with Spectral Acceleration Approach (SAA), which can effectively solve the electromagnetic scattering problem of layered rough surface. In this article, the electric field integral equations (EFIE) for layered rough surfaces is established, and the traditional forward and backward method (FBM) is introduced. Then, based on the traditional FBM algorithm, an Improved Generalized Forward and Backward Method is proposed and, by using the SAA technique in its iterative process, the computation of matrix-vector multiplication is accelerated, thus enabling rapid solution. In the algorithm validation, the same rough surface was calculated using the MoM, FBM, and IGFBM-SAA. The study found that when root mean square (RMS) heights are $h_1 = h_2 = 0.1\lambda$, the convergence accuracy can reach $\tau = 10^{-7}$ after 14 iterations. However, as the roughness increases to $h_1 = h_2 = 0.3\lambda$ and $h_1 = h_2 = 0.5\lambda$, the convergence accuracy falling to $\tau = 10^{-5}$ and $\tau = 10^{-5}$, respectively. This indicates that it is necessary to adjust the integration parameters to improve the convergence accuracy. In addition, it was found that when the size of the rough surface is 25.6λ, the computational times for calculations are 91 s (IGFBM-SAA), 197 s (FBM), and 410 s (MoM), respectively. When the size of the rough surface increases to 51.2λ, the computational time differences become more significant, with 236 s, 756 s, and 2547 s being the respective values. This indicates that the proposed algorithm in this article has significant computational speed advantages when dealing with larger rough surfaces. Based on this algorithm, this article studied the electromagnetic scattering characteristics of layered rough surfaces with different parameters (RMS height, dielectric constant, and correlation length), and relevant research results can provide valuable references for areas such as radar target recognition and radar stealth technology, thereby enhancing the accuracy and reliability of radar detection as well as radar stealth performance.

Index Terms – electric field integral equations, electromagnetic scattering, Improved Generalized Forward and Backward Method, layered rough surface, Spectral Acceleration Approach.

I. INTRODUCTION

Rough surface electromagnetic scattering has important application value in radar remote sensing and communication fields. In practical applications, accurately predicting and modeling the electromagnetic scattering characteristics of rough surfaces have shown important practical significance for optimizing radar image interpretation and improving the performance of communication systems. However, despite the existence of some classical methods such as the large-scale Kirchhoff approximation [1–4], the small-scale perturbation method [5–8], and the general Rayleigh method [9–11], these methods typically rely on certain simplifying assumptions, have limited applicability, and impose specific limitations on the parameters of the rough surface. Therefore, studying computation methods for rough surface electromagnetic scattering with universal applicability and high accuracy has important theoretical and practical significance.

In recent years, with the continuous development of computer technology, numerical calculation methods such as the method of moment (MoM) [12–15], the finite difference time domain method (FDTD) [16–19], and the finite element method (FEM) [20–22] have been widely used in the study of rough surface electromagnetic scattering. These methods can provide high-precision calculation results and have no specific limitations on the parameters of the rough surface. However, because numerical methods require discretizing the rough surface, the resulting unknowns are numerous, leading to high computational complexity. Currently, most numerical methods have a computational cost that grows cubically with the number of unknowns ($o(N^3)$) when dealing with rough surface electromagnetic scattering problems, which limits their practical applications to some extent.

Submitted On: September 28, 2023
Accepted On: January 12, 2024

https://doi.org/10.13052/2024.ACES.J.390202

In addition, accurate calculation of rough surface electromagnetic scattering requires not only high-precision numerical calculation methods but also efficient numerical optimization techniques. Although many researchers have conducted extensive and in-depth research in this field, there are still many problems that need to be addressed, for example how to improve computational accuracy and efficiency.

Article [23] mainly investigated the electromagnetic scattering problem based on the composite rough surface modeling method and the improved SBR-FBSSA algorithm. They placed objects in a canyon/valley environment and analyzed the electromagnetic scattering characteristics of that environment. This study extended the environmental complexity of scattering research by applying the composite rough surface modeling method and the improved SBR-FBSSA algorithm to solve the electromagnetic scattering problems in canyon/valley environments. Article [24] proposed an efficient and accurate method using the MoM-SMCG method combined with adaptive integration to solve the electromagnetic scattering problem of random rough surfaces. The main contribution of this work included using MoM to calculate the electromagnetic scattering coefficients of rough surfaces, and then using the adaptive selection integration point method (SMCG) to integrate and solve the electromagnetic scattering of rough surfaces. This study applied the MoM-SMCG method to the electromagnetic scattering problem of random rough surfaces, improving the computational efficiency and accuracy. Article [25] used the discrete two-level complex image method (DSCM) to calculate the electromagnetic scattering of completely conducting periodic rough surfaces. A model of completely conducting periodic rough surfaces was established and DSCM was used to calculate the electromagnetic scattering coefficients of rough surfaces. Then, the FDTD method was used to solve the electromagnetic scattering problems of rough surfaces. This study applied DSCM to the electromagnetic scattering problems of completely conducting periodic rough surfaces, improving the understanding of these scattering problems. Article [26] mainly studied an innovative method in the engineering field, the hybrid AMCFFM-MAE method, which can quickly simulate the electromagnetic scattering of one-dimensional rough surfaces over a frequency band. The importance of this research lies in that it provides a new engineering tool to better understand and solve practical electromagnetic scattering problems involving rough surfaces. Article [27] proposed a hybrid method for solving the composite scattering problem of targets and rough ground. The uniqueness of this method lies in that it combines the physical optics method and physical basis function method, which can accurately simulate and solve the electromagnetic scattering characteristics of rough surfaces. This study has made important extensions and improvements to the application of physical optics methods in complex environments. Article [28] proposed a fast algorithm mainly for calculating the electromagnetic scattering of one-dimensional rough surfaces. This algorithm is based on integral equation methods and basis function expansion methods, and can effectively simulate the electromagnetic scattering characteristics of complex rough surfaces. The development of this algorithm provides important theoretical basis and practical guidance for understanding and solving electromagnetic scattering problems involving rough surfaces in practical environments. Compared to that, the layered rough surfaces studied in this paper are more common in nature, such as the surface of a sea covered with floating ice, ground covered with snow or leaves, etc. Therefore, studying the electromagnetic scattering characteristics of layered rough surfaces is of great significance. However, the computational volume for calculating layered rough surfaces using numerical methods is very large, so fast algorithms need to be applied. The algorithm proposed in this paper can effectively solve this problem and save a lot of time, improving computational efficiency. This advantage is more prominent when the rough surface length is large.

This article proposes an efficient Improved Generalized Forward and Backward Method-Spectral Acceleration Approach (IGFBM-SAA) algorithm for electromagnetic scattering from layered rough surfaces, aiming to improve computational efficiency and thereby enhance research efficiency. Firstly, an electric field integral equation (EFIE) for layered rough surfaces is established, and the traditional forward and backward method (FBM) is modified to propose the innovative IGFBM method. At the same time, in order to reduce the error caused by the artificial truncation of the rough surface, a conical wave is used as the incident wave. This wave has Gaussian characteristics, which gradually decrease to zero as it approaches the boundary. This property effectively avoids the abrupt change of surface current, thereby improving the accuracy of the calculation. Then, SAA technology is combined to accelerate the calculation to achieve rapid solution. Subsequently, the computational results of the IGFBM-SAA algorithm are compared with those of MoM to verify the effectiveness and accuracy of the proposed algorithm. Finally, the electromagnetic scattering characteristics of different layered rough surfaces are studied through several examples. The results show that the IGFBM-SAA algorithm has significant advantages when calculating scattering from long layered rough surfaces. The research findings in this article have positive contributions to the technological progress in areas such as target recogni-

tion, target detection, radar stealth, and other related fields.

II. IGFBM-SAA FAST ALGORITHM MODEL

Ground covered with leaves or snow, grassland, and the sea surface covered with ice chunks can all be regarded as layered rough media surfaces. Therefore, studying the composite scattering of layered rough media surfaces and targets has important significance.

A. Electric field integral equations (EFIE) for layered rough surface

The rough surface of the three-layer medium is shown in Fig. 1. The upper and lower rough surfaces divide the medium into three layers, with parameters (ε_0,μ_0), (ε_1,μ_1), and (ε_2,μ_2) for each region. The contour S_1 of the upper rough surface is represented by $z_1=f_1(x)$, and the contour S_2 of the lower rough surface is represented by $z_2=f_2(x)$. The incident field is ψ^{inc}. ψ_0, ψ_1, and ψ_2 represent the fields within each region of the medium, and they satisfy the following boundary equations:

$$\frac{\psi_0(\mathbf{r})}{2}-\int_{S_1}\left[\psi_0(\mathbf{r}')\frac{\partial G_0(\mathbf{r},\mathbf{r}')}{\partial \mathbf{n}'} -G_0(\mathbf{r},\mathbf{r}')\frac{\partial \psi_0(\mathbf{r}')}{\partial \mathbf{n}'}\right]ds'=\psi^{\mathrm{inc}}(\mathbf{r}) \quad \mathbf{r}\in S_1\ , \tag{1}$$

$$\frac{\psi_1(\mathbf{r}')}{2}-\int_{S_2}\left[\psi_1(\mathbf{r}')\frac{\partial G_1(\mathbf{r},\mathbf{r}')}{\partial \mathbf{n}'}-G_1(\mathbf{r},\mathbf{r}')\frac{\partial \psi_1(\mathbf{r}')}{\partial \mathbf{n}'}\right]ds' +\int_{S_1}\left[\psi_1(\mathbf{r}')\frac{\partial G_1(\mathbf{r},\mathbf{r}')}{\partial \mathbf{n}'}-G_1(\mathbf{r},\mathbf{r}')\frac{\partial \psi_1(\mathbf{r}')}{\partial \mathbf{n}'}\right]ds'=0 \tag{2}$$

$$\mathbf{r}\in S_1 \text{ or } \mathbf{r}\in \mathrm{S}_2,$$

$$\frac{\psi_2(\mathbf{r})}{2}+\int_{S_2}\psi_2(\mathbf{r}')\frac{\partial G_2(\mathbf{r},\mathbf{r}')}{\partial \mathbf{n}'}-G_2(\mathbf{r},\mathbf{r}')\frac{\partial \psi_2(\mathbf{r})}{\partial \mathbf{n}'}ds'=0 \quad \mathbf{r}\in S_2, \tag{3}$$

where $\int_S$ represents the integration over the rough surface, $G_0(\mathbf{r},\mathbf{r}')$ represents the Green's function in free space, and $G_1(\mathbf{r},\mathbf{r}')$ and $G_2(\mathbf{r},\mathbf{r}')$ represent the Green's functions in medium 1 and medium 2, respectively. At the same time, the fields in each region satisfy the following boundary conditions:

$$\psi_i(\mathbf{r})=\psi_{i+1}(\mathbf{r}), \tag{4}$$

$$\frac{\partial \psi_{i+1}(\mathbf{r})}{\partial n}=\rho\frac{\partial \psi_i(\mathbf{r})}{\partial n}\ \ (i=0,1). \tag{5}$$

For TE wave, $\rho=\mu_{i+1}/\mu_i$. For TM wave, $\rho=\varepsilon_{i+1}/\varepsilon_0$.

Assuming that the length of the rough surface is L and the discrete density Δx is uniform, equations (1-3) can be simplified as follows:

$$\mathbf{A}^{(0,1,1)}U_1+\mathbf{B}^{(0,1,1)}\psi_1=\psi^{inc}, \tag{6}$$

$$\rho_1\mathbf{A}^{(1,1,1)}U_1+\mathbf{B}^{(1,1,1)}\psi_1+\mathbf{A}^{(1,1,2)}U_2+\mathbf{B}^{(1,1,2)}\psi_2=0, \tag{7}$$

$$\rho_1\mathbf{A}^{(1,2,1)}U_1+\mathbf{B}^{(1,2,1)}\psi_1+\mathbf{A}^{(1,2,2)}U_2+\mathbf{B}^{(1,2,2)}\psi_2=0, \tag{8}$$

$$\rho_2\mathbf{A}^{(2,2,2)}U_2+\mathbf{B}^{(2,2,2)}\psi_2=0. \tag{9}$$

The expression for each matrix element is as follows [29]:

$$\mathbf{A}_{mn}^{(a,b,c)}=\begin{cases} w^{(a,c)}\frac{i\Delta x}{4}H_0^{(1)}\left(k_a\left|\mathbf{r}_{m,b}-\mathbf{r}_{n,c}\right|\right)\Delta l_{m,b} \\ \quad (b=c,m\neq n) \text{ or } b\neq c \\ w^{(a,c)}\frac{i\Delta x}{4}\left[1+\frac{i2}{\pi}\ln\left(\frac{e^{\gamma}k_a\Delta x\Delta l_{m,b}}{4e}\right)\right] \\ \quad (b=c,m=n) \end{cases}, \tag{10}$$

$$\mathbf{B}_{mn}^{(a,b,c)}=\begin{cases} -w^{(a,c)}\frac{ik_a\Delta x}{4}\frac{H_1^{(1)}\left(k_a\left|\mathbf{r}_{m,b}-\mathbf{r}_{n,c}\right|\right)}{\left|\left|\mathbf{r}_{m,b}-\mathbf{r}_{n,c}\right|\right|}\times \\ (f_c'(x_n)(x_n-x_m)-(f_c(x_n)-f_b(x_m))) \\ \quad (b=c,m\neq n) \text{ or } b\neq c \\ \frac{1}{2}-w^{(a,c)}\frac{f_b''(x_m)}{4\pi}\frac{\Delta x}{1+f_b'(x_m)^2} \\ \quad (b=c,m=n) \end{cases}, \tag{11}$$

where

$$w^{(a,c)}=\begin{cases} 1 & a=c \\ -1 & a\neq c \end{cases}, \tag{12}$$

$$U_{i,m}=\sqrt{1+(f_i'(x_m))^2}\,\partial\psi_i(x_m)\Big/\partial n\ \ (i=1,2,3)\ . \tag{13}$$

In the equations above, the first superscript indicates the region, the second superscript indicates the roughness location where the field point is located, and the third superscript indicates the roughness location where the source point is located.

Therefore, equations (6-9) can be transformed into a matrix equation:

$$\begin{bmatrix} \mathbf{A}^{(0,1,1)} & \mathbf{B}^{(0,1,1)} & 0 & 0 \\ \rho_1\mathbf{A}^{(1,1,1)} & \mathbf{B}^{(1,1,1)} & \mathbf{A}^{(1,1,2)} & \mathbf{B}^{(1,1,2)} \\ \rho_1\mathbf{A}^{(1,2,1)} & \mathbf{B}^{(1,2,1)} & \mathbf{A}^{(1,2,2)} & \mathbf{B}^{(1,2,2)} \\ 0 & 0 & \rho_2\mathbf{A}^{(2,2,2)} & \mathbf{B}^{(2,2,2)} \end{bmatrix}\cdot\begin{bmatrix} \mathbf{U}_1 \\ \psi_1 \\ \mathbf{U}_2 \\ \psi_2 \end{bmatrix}=\begin{bmatrix} \psi^{inc} \\ 0 \\ 0 \\ 0 \end{bmatrix}. \tag{14}$$

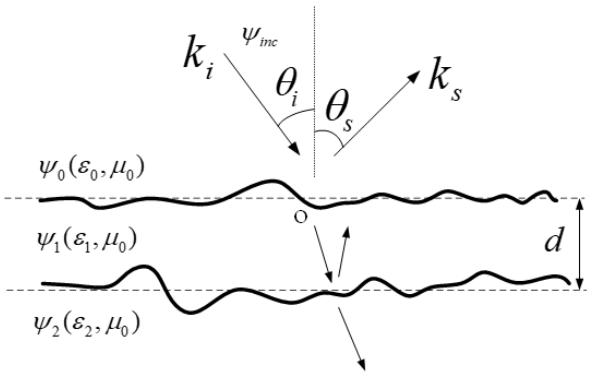

Fig. 1. Schematic diagram of layered rough surface.

B. Forward and backward method (FBM)

Solving scattering problems using numerical algorithms ultimately requires transforming them into matrix equation solutions:

$$\mathbf{ZI} = \mathbf{V}, \tag{15}$$

where $\boldsymbol{Z}$ is the impedance matrix, $\boldsymbol{V}$ is the excitation vector, and $\boldsymbol{I}$ is the unknown vector to be solved. The traditional method for solving this system is to invert the impedance matrix, which requires a computational cost and storage cost of $o(N^3)$ (where N is the number of unknowns). When the number of unknowns is large, this approach requires significant memory and computation time.

FBM [29–31] has good convergence properties for problems involving scattering from rough surfaces. It divides the induced current of each discrete element on the rough surface into forward and backward contributions to the scattering field. The forward contribution is generated by the incident electromagnetic wave and the induced current of the source element located in front of the receiving field element, while the backward contribution is generated by the induced current of the source element located behind the receiving field element. The calculation process follows.

First, divide the impedance matrix into three matrices:

$$\mathbf{Z} = \mathbf{Z}_f + \mathbf{Z}_s + \mathbf{Z}_b. \tag{16}$$

Among them, $\mathbf{Z}_f$ is a lower triangular matrix representing the contributions of all source currents located before the receiving unit, $\mathbf{Z}_b$ is an upper triangular matrix representing the contributions of all source currents located behind the receiving unit, and $\mathbf{Z}_s$ is a diagonal matrix representing the contributions of each point on the rough surface to itself.

Divide the unknown vector $\boldsymbol{I}$ to be solved into two parts:

$$\mathbf{I} = \mathbf{I}_f + \mathbf{I}_b, \tag{17}$$

where $\boldsymbol{I}_f$ is the induced current on the rough surface contributing to the forward propagation of electromagnetic waves, and $\boldsymbol{I}_b$ is the induced current on the rough surface contributing to the backward propagation of electromagnetic waves.

The following equation system can be obtained from the three equations above:

$$\mathbf{Z}_s\mathbf{I}_f = \mathbf{Z} - \mathbf{Z}_f\left[\mathbf{I}_f + \mathbf{I}_b\right], \tag{18}$$

$$\mathbf{Z}_s\mathbf{I}_b = -\mathbf{Z}_b\left[\mathbf{I}_f + \mathbf{I}_b\right]. \tag{19}$$

It can be transformed into the following iterative form:

$$\left[\mathbf{Z}_s + \mathbf{Z}_f\right]\mathbf{I}_f^{(n)} = \mathbf{Z} - \mathbf{Z}_f\mathbf{I}_b^{(n-1)}, \tag{20}$$

$$\left[\mathbf{Z}_s + \mathbf{Z}_b\right]\mathbf{I}_b^{(n)} = -\mathbf{Z}_b\mathbf{I}_f^{(n)}. \tag{21}$$

Define the convergence accuracy as follows:

$$\tau = \frac{\mathbf{Z}\left[(\mathbf{I}_f^{(n)} + \mathbf{I}_b^{(n)}) - (\mathbf{I}_f^{(n-1)} + \mathbf{I}_b^{(n-1)})\right]}{\mathbf{Z}} < \varepsilon. \tag{22}$$

The iterative process starts with $\mathbf{I}_b^{(0)} = 0$ as the initial value, and first calculates $\mathbf{I}_f^{(1)}$ using equation (20), then calculates $\mathbf{I}_b^{(1)}$ using equation (21). This process iterates until the specified convergence accuracy is met. The computational cost of this algorithm is $o(N^2)$, and it has fast convergence speed, making it an effective algorithm for solving scattering problems of rough surfaces.

However, if we want to use FBM to solve the matrix equation (14), we need to improve the FBM method. Next, we will introduce IGFBM.

C. Improved Generalized Forward and Backward Method (IGFBM)

Decompose the impedance matrix into upper, lower, and diagonal matrices denoted by U, L, and D, respectively. For example, the submatrix denoted by (l,l,l) has the following form:

$$\mathbf{A}^{(l,l,l)} = \mathbf{A}^{\mathrm{U},(l,l,l)} + \mathbf{A}^{\mathrm{L},(l,l,l)} + \mathbf{A}^{\mathrm{D},(l,l,l)}, \tag{23}$$

$$\mathbf{B}^{(l,l,l)} = \mathbf{B}^{\mathrm{U},(l,l,l)} + \mathbf{B}^{\mathrm{L},(l,l,l)} + \mathbf{B}^{\mathrm{D},(l,l,l)}. \tag{24}$$

The unknown vector is decomposed into forward and backward components, $\mathbf{U}_i = \mathbf{U}_i{}^{\mathrm{f}} + \mathbf{U}_i{}^{\mathrm{b}}$ and $\psi_i = \psi_i{}^{\mathrm{f}} + \psi_i{}^{\mathrm{b}}$, where $\mathbf{U}_i{}^{\mathrm{f}}$ and $\psi_i{}^{\mathrm{f}}$ are the forward components, and $\mathbf{U}_i{}^{\mathrm{b}}$ and $\psi_i{}^{\mathrm{b}}$ are the backward components. Therefore, the forward current iteration formula in equation (14) is written as:

$$\begin{aligned}\mathbf{A}^{\mathrm{L},(0,1,1)}\mathbf{U}_1^{\mathrm{f}} + \mathbf{B}^{\mathrm{L},(0,1,1)}\psi_1^{\mathrm{f}} &= \psi^{inc} \\ &- \mathbf{A}^{\mathrm{D},(0,1,1)}(\mathbf{U}_1^{\mathrm{f}} + \mathbf{U}_1^{\mathrm{b}}) - \mathbf{B}^{\mathrm{D},(0,1,1)}(\psi_1^{\mathrm{f}} + \psi_1^{\mathrm{b}}),\end{aligned} \tag{25}$$

$$\begin{aligned}\rho_1\mathbf{A}^{\mathrm{L},(1,1,1)}\mathbf{U}_1^{\mathrm{f}} + \mathbf{B}^{\mathrm{L},(1,1,1)}\psi_1^{\mathrm{f}} + \mathbf{A}^{\mathrm{L},(1,1,2)}\mathbf{U}_2^{\mathrm{f}} + \mathbf{B}^{\mathrm{L},(1,1,2)}\psi_2^{\mathrm{f}} \\ = -\rho_1\mathbf{A}^{\mathrm{D},(1,1,1)}(\mathbf{U}_1^{\mathrm{f}} + \mathbf{U}_1^{\mathrm{b}}) - \mathbf{B}^{\mathrm{D},(1,1,1)}(\psi_1^{\mathrm{f}} + \psi_1^{\mathrm{b}}) \\ - \mathbf{A}^{\mathrm{D},(1,1,2)}(\mathbf{U}_2^{\mathrm{f}} + \mathbf{U}_2^{\mathrm{b}}) - \mathbf{B}^{\mathrm{D},(1,1,2)}(\psi_2^{\mathrm{f}} + \psi_2^{\mathrm{b}}),\end{aligned} \tag{26}$$

$$\begin{aligned}\rho_1\mathbf{A}^{\mathrm{L},(1,1,1)}\mathbf{U}_1^{\mathrm{f}} + \mathbf{B}^{\mathrm{L},(1,1,1)}\psi_1^{\mathrm{f}} + \mathbf{A}^{\mathrm{L},(1,1,2)}\mathbf{U}_2^{\mathrm{f}} + \mathbf{B}^{\mathrm{L},(1,1,2)}\psi_2^{\mathrm{f}} \\ = -\rho_1\mathbf{A}^{\mathrm{D},(1,2,1)}(\mathbf{U}_1^{\mathrm{f}} + \mathbf{U}_1^{\mathrm{b}}) - \mathbf{B}^{\mathrm{D},(1,2,1)}(\psi_1^{\mathrm{f}} + \psi_1^{\mathrm{b}}) \\ - \mathbf{A}^{\mathrm{D},(1,2,2)}(\mathbf{U}_2^{\mathrm{f}} + \mathbf{U}_2^{\mathrm{b}}) - \mathbf{B}^{\mathrm{D},(1,2,2)}(\psi_2^{\mathrm{f}} + \psi_2^{\mathrm{b}}),\end{aligned} \tag{27}$$

$$\begin{aligned}\rho_2\mathbf{A}^{\mathrm{L},(2,2,2)}\mathbf{U}_1^{\mathrm{f}} + \mathbf{B}^{\mathrm{L},(2,2,2)}\psi_1^{\mathrm{f}} = \\ - \rho_2\mathbf{A}^{\mathrm{D},(2,2,2)}(\mathbf{U}_2^{\mathrm{f}} + \mathbf{U}_2^{\mathrm{b}}) - \mathbf{B}^{\mathrm{D},(2,2,2)}(\psi_2^{\mathrm{f}} + \psi_2^{\mathrm{b}}).\end{aligned} \tag{28}$$

The iterative formula for obtaining the backward current can be obtained analogously. By iterative solution, the unknown variables at the i-th iteration are $\mathbf{U}_1^{\mathrm{f},(i)}$, $\mathbf{U}_1^{\mathrm{b},(i)}$, $\psi_1^{\mathrm{f},(i)}$, $\psi_1^{\mathrm{b},(i)}$, $\mathbf{U}_2^{\mathrm{f},(i)}$, $\mathbf{U}_2^{\mathrm{b},(i)}$, $\psi_2^{\mathrm{f},(i)}$, $\psi_2^{\mathrm{b},(i)}$, and the iterative algorithm starts with initial values of $\mathbf{U}_1^{\mathrm{b},(0)} = 0$, $\psi_1^{\mathrm{b},(0)} = 0$, $\mathbf{U}_2^{\mathrm{b},(0)} = 0$, and $\psi_2^{\mathrm{b},(0)} = 0$, and calculates iteratively until the specified convergence accuracy is reached.

For the forward iteration process of IGFBM, the matrix-vector multiplication needs to be repeated, and

the process can be expressed as:

$$V_f^{(1)}(\mathbf{r}_n)=\sum_{m=1}^{n-1}A_{\mathrm{mn}}^{(0,1,1)}\cdot U_{1,m}+\sum_{m=1}^{n-1}B_{\mathrm{mn}}^{(0,1,1)}\cdot\psi_{1,m}, \tag{29}$$

$$V_f^{(2)}(\mathbf{r}_n)=\sum_{m=1}^{n-1}A_{\mathrm{mn}}^{(1,1,1)}\cdot \mathrm{U}_{1,m} + \sum_{m=1}^{n-1}B_{\mathrm{mn}}^{(1,1,1)}\cdot\psi_{1,m}+\sum_{m=1}^{n-1}A_{\mathrm{mn}}^{(1,1,2)}\cdot U_{2,m}+\sum_{m=1}^{n-1}B_{\mathrm{mn}}^{(1,1,2)}\cdot\psi_{2,m}, \tag{30}$$

$$V_f^{(3)}(\mathbf{r}_n)=\sum_{m=1}^{n-1}A_{\mathrm{mn}}^{(1,2,1)}\cdot U_{1,m}+\sum_{m=1}^{n-1}B_{\mathrm{mn}}^{(1,2,1)}\cdot\psi_{1,m} + \sum_{m=1}^{n-1}A_{\mathrm{mn}}^{(1,2,2)}\cdot U_{2,m}+\sum_{m=1}^{n-1}B_{\mathrm{mn}}^{(1,2,2)}\cdot\psi_{2,m}, \tag{31}$$

$$V_f^{(4)}(\mathbf{r}_n)=\sum_{m=1}^{n-1}A_{\mathrm{mn}}^{(2,2,2)}\cdot U_{1,m}+\sum_{m=1}^{n-1}B_{\mathrm{mn}}^{(2,2,2)}\cdot\psi_{1,m}, \tag{32}$$

where $n=1,2,...,N$. $V_f^{(i)}(\mathbf{r}_n)$ $(i=1,2,3,4)$ represents the radiation contribution generated by the source current in the n-th receiving element upstream of the interface, and the computational effort required for each iteration is $o(N^2)$. Therefore, the SAA algorithm can be used to accelerate the calculation and improve computational efficiency.

D. Spectral Acceleration Approach (SAA)

If SAA is applied to the calculation of equation (29), both the computational load and memory requirements are reduced to $o(N)$. The basic principle is to define a neighboring region L_s, where if a source element and a receiver element are within a certain distance, they are referred to as strong interaction group and produce strong interaction V_s, otherwise they are referred to as weak interaction group and produce weak interaction V_w. Equation (29) can be rewritten as:

$$V_f^{(1)}(\mathbf{r}_n)=V_s^{(1)}+V_w^{(1)}=\sum_{m=n-N_s}^{n-1}(A_{mn}^{(1,1,1)}\cdot U_{1,m}+B_{mn}^{(1,1,1)}\cdot\psi_{1,m}) + \sum_{m=1}^{n-N_s-1}(A_{mn}^{(1,1,1)}\cdot U_{1,m}+B_{mn}^{(1,1,1)}\cdot\psi_{1,m}). \tag{33}$$

The $V_s^{(1)}$ at position r_n is the contribution from the collective action of N_s source elements within a distance L_s of the field element receiving at position r_n, computed accurately using MOM. The contribution $V_w^{(1)}$ is from the collective action of $n-N_s-1$ source elements outside a distance L_s, which involves a large computational cost and reduces computational efficiency. Next, we discuss acceleration methods for this contribution.

Based on the spectral integral form of the Green's function [32], we can derive:

$$V_w^{(1)}(\mathbf{r}_n)=\sum_{m=1}^{n-N_s-1}(A_{mn}^{(1,1,1)}\cdot U_{1,m}+B_{mn}^{(1,1,1)}\cdot\psi_{1,m}) =\frac{i\Delta x}{4\pi}\int_{C_\theta}F_n(\theta)\exp(ik_1z_{1,n}\sin\theta)d\theta, \tag{34}$$

$$F_n(\theta)=F_{n-1}(\theta)\cdot\exp(ik_1\Delta x\cos\theta) + [-ik_1(-\sin\theta+\xi_x\cos\theta)\psi_{1,n-N_s-1}+\mathrm{U}_{1,n-N_s-1}] \cdot\exp[ik_1(N_s+1)\Delta x\cos\theta]\cdot\exp[-ik_1z_{1,n-N_s-1}\sin\theta]. \tag{35}$$

Similarly, we can obtain the spectral integral forms of $V_w^{(2)}$, $V_w^{(3)}$, and $V_w^{(4)}$. C_θ is the integration path. It can be seen that the weak contributions of all far-field elements $F_n(\theta)$ are now continuously recursively calculated by equation (35), with slowly changing field modes on the integration path making the SAA algorithm efficient.

Due to the weak contribution of the far field on the longer rough surface, $F_n(\theta)$ tends to have a narrow main lobe and multiple narrow side lobes in the complex plane. The choice of the integration path in equation (35) can be considered from C_θ to C_δ, such that $F_n(\theta)$ has a slowly varying mode with C_δ. The efficiency of the SAA algorithm lies in this slowly varying far field mode. The parameters chosen in Fig. 2 are as follows [31]:

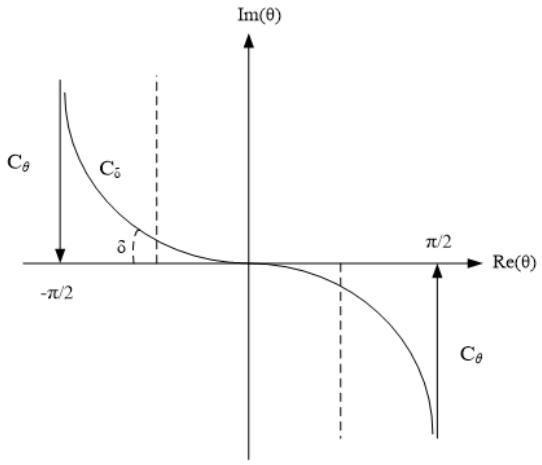

Fig. 2. Schematic diagram of spectral integration path.

where $\delta=\tan^{-1}(1/b)$, $b=\max(\sqrt{kR_s/20}\cdot\theta_s-1,1)$, $\theta_{s,\max}=\tan^{-1}(\frac{z_{\max}-z_{\min}+d}{R_s})$, $R_s=\sqrt{L_s^2+(z_{\max}-z_{\min}+d)^2}$.

Finally, choosing appropriate parameters, the discrete spectral integral form of the far-field can be obtained, for example, for A:

$$V_w^{(1)}=\frac{i\Delta xe^{-i\delta}}{4\pi}\sum_{p=-Q}^{Q}W(\theta_p)F_n(\theta_p)e^{ik_1z_{1,n}\sin\theta_p}\Delta\theta. \tag{36}$$

E. Conical incident wave

In simulation calculations, it is not practical to deal with the scattering of infinitely long rough surfaces, so the size of the rough surface is usually limited to a certain range. To avoid the effects of reflection and edge-bending caused by abrupt truncation of the rough surface edge, a conical incident wave [33] is used instead

of traditional plane wave incidence. This conical wave gradually decreases to zero as it approaches the boundary, effectively avoiding abrupt changes in surface current and significantly improving the accuracy of the calculation.

For the TE incident wave, the electromagnetic field expressions are:

$$\mathbf{E}_{inc}(\mathbf{r}) = \int_{-\infty}^{+\infty}\int_{-\infty}^{+\infty} \exp(\mathrm{j}k_x x + \mathrm{j}k_y y - \mathrm{j}k_z z) \cdot E(k_x,k_y)\, h_i(-k_z)\, dk_x dk_y, \tag{37}$$

$$\mathbf{H}_{inc}(\mathbf{r}) = -\frac{1}{\eta_0}\int_{-\infty}^{+\infty}\int_{-\infty}^{+\infty} \exp(\mathrm{j}k_x x + \mathrm{j}k_y y - \mathrm{j}k_z z) \cdot E(k_x,k_y)\, v_i(-k_z)\, dk_x dk_y. \tag{38}$$

For the TM incident wave, the electromagnetic field expressions are:

$$\mathbf{E}_{inc}(\mathbf{r}) = \int_{-\infty}^{+\infty}\int_{-\infty}^{+\infty} \exp(jk_x x + jk_y y - jk_z z) \cdot E(k_x,k_y)\, v_i(-k_z)\, dk_x dk_y, \tag{39}$$

$$\mathbf{H}_{inc}(\mathbf{r}) = -\frac{1}{\eta_0}\int_{-\infty}^{+\infty}\int_{-\infty}^{+\infty} \exp(jk_x x + jk_y y - jk_z z) \cdot E(k_x,k_y)\, h_i(-k_z)\, dk_x dk_y, \tag{40}$$

where $E(k_x,k_y)$ is the incident spectrum, $\mathbf{h}_i$ is the horizontal polarization direction, v_i is the vertical polarization direction, η_0 is the free space wave impedance, and k_i is the spatial spectral domains in the i directions, respectively, $k_\rho = \sqrt{k_x^2 + k_y^2}$.

The two-dimensional normalized conical incident wave amplitude is shown in Fig. 3. It can be seen from this that the magnetic field is strongest from the center of the rough surface and slowly returns to zero at the edges. Therefore, the tapered incident wave can be used to reduce the error caused by truncating the rough surface.

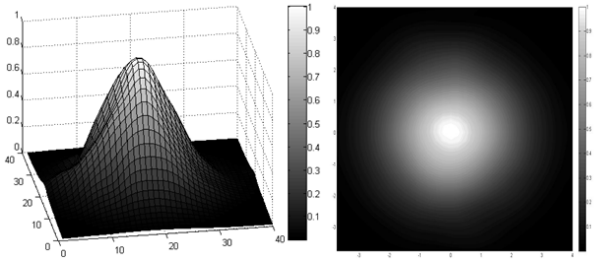

(a) (b)

Fig. 3. Normalized conical wave schematic.

III. VALIDATION OF ALGORITHM

Before applying the proposed IGFBM-SAA algorithm to practical situations, we need to verify its effectiveness and accuracy in calculating scattering from layered rough surfaces. To avoid overlap for different rough surfaces, all interfaces are modeled using Gaussian rough surfaces with the same parameters. The characteristics of these rough surfaces, including the root mean square (RMS) height and correlation length of the upper and lower layers, are described by parameters h_1, l_1, h_2, and l_2. In addition, we also need to consider the dielectric constants of the media, which are $\varepsilon_{r1} = 2.0 + i0.05$ and $\varepsilon_{r2} = 25 + i0$. Furthermore, we set the following parameters: rough surface length $L = 51.2\lambda$, correlation length $l_1 = l_2 = 1.0\lambda$, upper rough surface thickness $d = 10\lambda$, incident frequency $f = 1$ GHz, and incident angle $\theta_i = 60^\circ$.

In the verification process, we used this algorithm to calculate an example of scattering from a layered rough surface and stored the calculated results in Fig. 4. For comparison of the accuracy of the algorithm, we used traditional MoM as validation algorithms. This algorithm is relatively slow in calculation speed, but with high accuracy. We used MoM to calculate the same example and plotted the calculated results on the same graph for comparison.

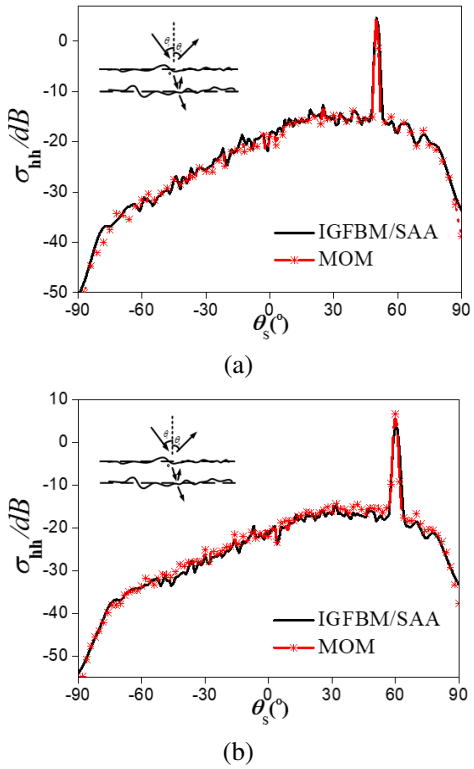

Fig. 4. Validation of algorithm: (a) horizontal polarization and (b) vertical polarization.

From Fig. 4 we can see that the calculated results of the three methods are in good agreement, which indicates that the IGFBM-SAA algorithm is effective in calculating scattering from layered rough surfaces.

To more accurately evaluate the performance of the algorithm, we used different rough surface lengths, 12.8λ, 25.6λ, and 51.2λ, corresponding to different dimensions of the impedance matrix, 512, 1024, and 2048, respectively. Other parameters were kept constant. Then we compared the computational time of the IGFBM-SAA algorithm with that of FBM and MoM. To ensure accurate statistical analysis, we averaged the time taken for 20 calculations. As shown in Fig. 5, we conducted a detailed comparison between the IGFBM/SAA algorithm, traditional MoM, and FBM. The results showed that the IGFBM/SAA algorithm exhibited significant advantages in computational speed compared to traditional MoM and FBM. This advantage was even more pronounced when dealing with large-scale rough surfaces. This enabled the algorithm to complete tasks more efficiently when dealing with large-scale rough surface scattering problems, providing strong support for practical engineering applications.

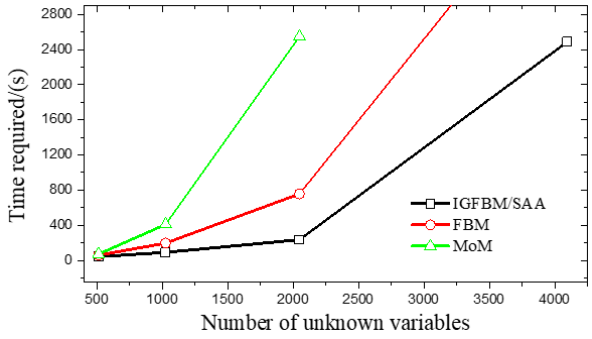

Fig. 5. Computational time.

During the above computations and validation process, we used a simulation computer with a CPU frequency of 3.4 GHz and 8 GB of memory. These parameters are sufficient for running large-scale rough surface scattering calculations. However, for more complex or larger-scale computational requirements, higher-performance computers or parallel computing techniques may be required to meet computational needs.

We conducted research on the convergence performance of this algorithm for different values of rough surface RMS height. As shown in Fig. 6 (a), when TE wave is incident, the algorithm achieves $\tau = 10^{-7}$ after 14 iterations when the roughness is $h_1 = h_2 = 0.1\lambda$, and the error increases to $\tau = 10^{-5}$ after the same number of iterations when the roughness is $h_1 = h_2 = 0.3\lambda$. However, when the roughness is $h_1 = h_2 = 0.5\lambda$, the convergence accuracy can only reach $\tau = 10^{-3}$, indicating that as the roughness increases, the convergence performance of IGFBM-SAA decreases. This is mainly due to the increase in error in solving spectral integral equation

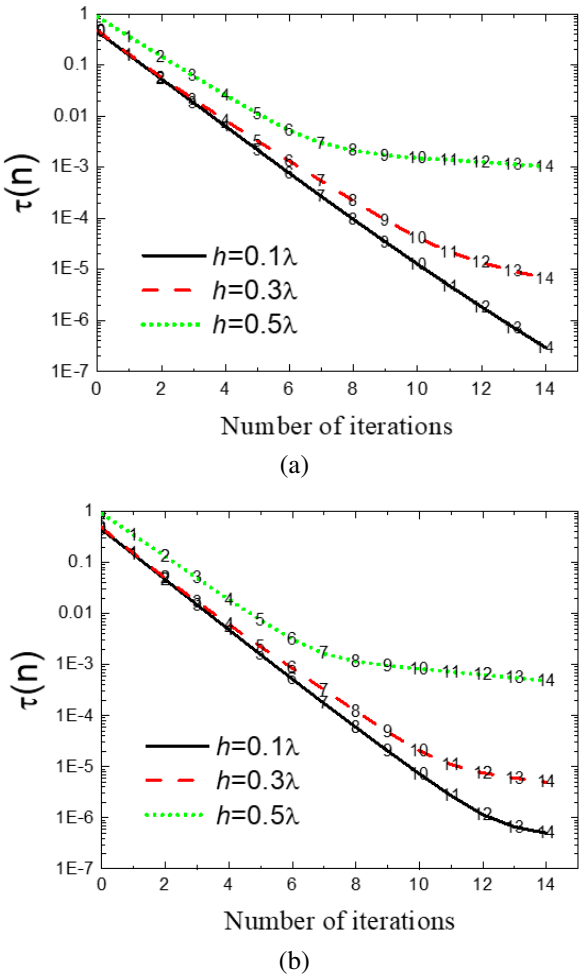

Fig. 6. Algorithmic convergence analysis chart: (a) TE incident wave and (b) TM incident wave.

(36) with increasing roughness. To improve the convergence accuracy, it is necessary to reselect integral parameters. In addition, it was found that the characteristics of TM wave incidence are different from those of TE wave incidence. As shown in Fig. 6 (b), it can be clearly seen that the convergence speed of TM wave is faster, but its convergence accuracy is lower than that of TE wave incidence.

In summary, when studying rough surface scattering problems, appropriate algorithms and parameter settings need to be carefully selected for different incident waves and roughness to ensure good convergence performance and computational accuracy of the algorithm. Especially when the roughness increases, it may be necessary to readjust parameters of the algorithm to reduce the error in spectral integral solution and improve convergence accuracy. This finding has important guiding significance for practical applications in dealing with complex rough surface scattering problems.

IV. CALCULATION RESULTS AND ANALYSIS

This section mainly studies and analyzes the electromagnetic scattering characteristics of layered rough surfaces under different parameters. Unless otherwise specified, the relevant parameters are set as: dielectric constants of the media $\varepsilon_{r1} = 2.0 + i0.05$ and $\varepsilon_{r2} = 25 + i0$, rough surface length $L = 51.2\lambda$, $h_1 = h_2 = 0.2\lambda$, correlation length $l_1 = l_2 = 1.0\lambda$, upper rough surface thickness $d = 6\lambda$, incident frequency $f = 1GHz$, and incident angle $\theta_i = 40^\circ$.

Figure 7 demonstrates the impact of changes in the RMS height of a layered rough surface on the bistatic scattering coefficient under TM wave incidence, with RMS heights chosen as $h_1 = h_2 = 0.2$, $h_1 = h_2 = 0.5$, and $h_1 = h_2 = 1.0$, respectively. The correlation length of the rough surface follows $l_1 = l_2 = 1.0\lambda$, and the incident angle is $\theta_i = 40^\circ$. Upon close examination, it is observed that the bistatic scattering coefficient of the layered rough surface tends to decrease in the specular direction with increasing RMS height, particularly evident when the RMS height is $h_1 = h_2 = 0.2$ and $h_1 = h_2 = 0.5$. Conversely, in the non-specular scattering directions, the bistatic scattering coefficient increases with increasing RMS height, particularly prominent when the RMS height is $h_1 = h_2 = 1.0$. Additionally, compared to the specular direction, the bistatic scattering coefficient is generally smaller in the non-specular directions, indicating a stronger scattering ability of the layered rough surface in the specular direction.

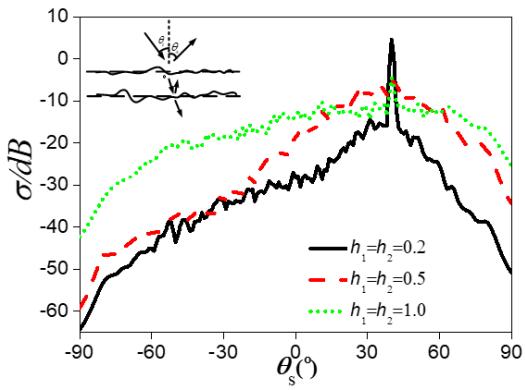

Fig. 7. Scattering coefficient comparison chart for different root mean square (RMS) heights.

This observed phenomenon indicates that the RMS height of rough surfaces has a significant impact on bistatic scattering coefficients that depends on the direction of scattering. This finding can provide valuable reference and applications in areas such as electromagnetic scattering and radar target characterization. For example, in radar target recognition, by studying the scattering characteristics of layered rough surfaces, targets can be identified and classified more accurately, thereby enhancing the accuracy and reliability of radar detection. Additionally, in radar stealth technology, surface structures with lower scattering coefficients can be designed and implemented based on studies of layered rough surfaces to decrease the probability of targets being detected by radar, thus enhancing their radar stealth performance. Furthermore, this research can also be applied to electromagnetic compatibility analysis and prediction.

Figure 8 shows the dependence of the scattering coefficient of a layered rough surface on the correlation length when TM wave incidence. As seen from the figure, the scattering coefficient increases with increasing correlation length in the specular direction. However, at large scattering angles, the scattering coefficient decreases with increasing correlation length. This observation is consistent with the conclusions of many electromagnetic scattering studies, indicating that the scattering characteristics of rough surfaces are not only determined by their surface structure but also affected by the incident conditions of electromagnetic waves.

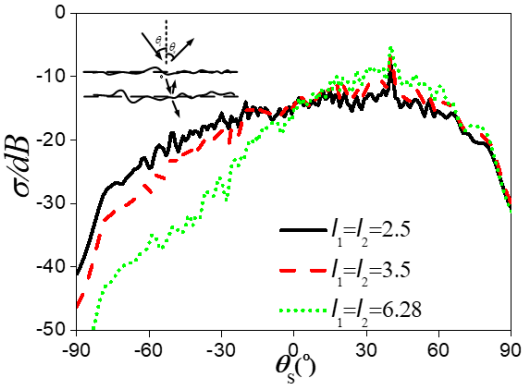

Fig. 8. Scattering coefficient comparison chart for different correlation lengths.

In the specular direction, as the correlation length increases, the details and fluctuations of the surface structure become more significant, which leads to an increase in the scattering coefficient. This trend can be understood as follows: as the surface structure changes, the complexity of scattering increases, causing more electromagnetic energy to be scattered into different directions.

However, in the region of large scattering angles, the situation is different. In this region, the decrease in scattering coefficient is related to the increase in surface structure size and the propagation characteristics of electromagnetic waves. More specifically, when electromagnetic waves propagate from regions with larger surface structures, the coherence of the wave may be affected,

leading to a decrease in scattering coefficient. Additionally, larger surface structures may provide more propagation paths for electromagnetic waves, causing some waves to bypass the surface structure rather than undergo strong scattering.

In the subsequent study, we applied the IGFBM-SAA method to deeply explore the impact of the changes in the dielectric constant ε_2 of the lower rough surface on electromagnetic scattering coefficients. In the simulation calculations, both the upper and lower media were lossless, with the dielectric constant of the upper medium being $\varepsilon_1 = 5.0$ and the dielectric constants of the lower media being $\varepsilon_2 = 5.0$, $\varepsilon_2 = 10.0$, and $\varepsilon_2 = 20.0$, respectively. The rms and correlation length of the upper-lower interface were $h_1 = h_2 = 0.5$ and $l_1 = l_2 = 1.0\lambda$, respectively, and the incident angle was $\theta_i = 40°$.

To visually present the changes in the scattering coefficients, we plotted Fig. 9 (a), which demonstrated the trend of the scattering coefficient varying with the dielectric constant ε_2 throughout the entire scattering angle range. It could be clearly observed from the figure that with the increase in the dielectric constant ε_2, the scattering coefficient changed at each scattering angle but this change was not monotonous. At some specific scattering angles, a significant peak was observed in the scattering coefficient; at other angles, it might decrease. This complex trend reflected the complex impact of the dielectric constant ε_2 on the scattering process.

To better reveal the changing rules of the scattering coefficient with respect to the dielectric constant, we plotted Fig. 9 (b), which presented the changes in the scattering coefficient within the scattering angle range -90°∼75°. In particular, when the dielectric constant was $\varepsilon_2 = 5.0$, the electromagnetic scattering of the layered rough surface would simplify to that of a single rough surface. It could be seen from Fig. 9 (b) that at large scattering angles, the scattering coefficient of the layered rough surface was always greater than that of a single rough surface. Additionally, with the increase in $|\varepsilon_1 - \varepsilon_2|$, the scattering coefficient of the layered rough surface also showed an increasing trend. This trend might be attributed to the gradually enhanced scattering effect of electromagnetic waves by the lower medium as $|\varepsilon_1 - \varepsilon_2|$ increased.

In summary, through applying the IGFBM-SAA method, we conducted an in-depth investigation into the impact of changes in the dielectric constant on the scattering process of rough surfaces. The investigation revealed that, regardless of how the dielectric constant changed, the scattering coefficient of the layered rough surface at some specific scattering angles was always greater than that of a single rough surface. Especially at large scattering angles, the scattering coefficient of the layered rough surface showed an increasing trend. This trend might be because the layered rough surface exhibits more complex scattering characteristics during the propagation of electromagnetic waves.

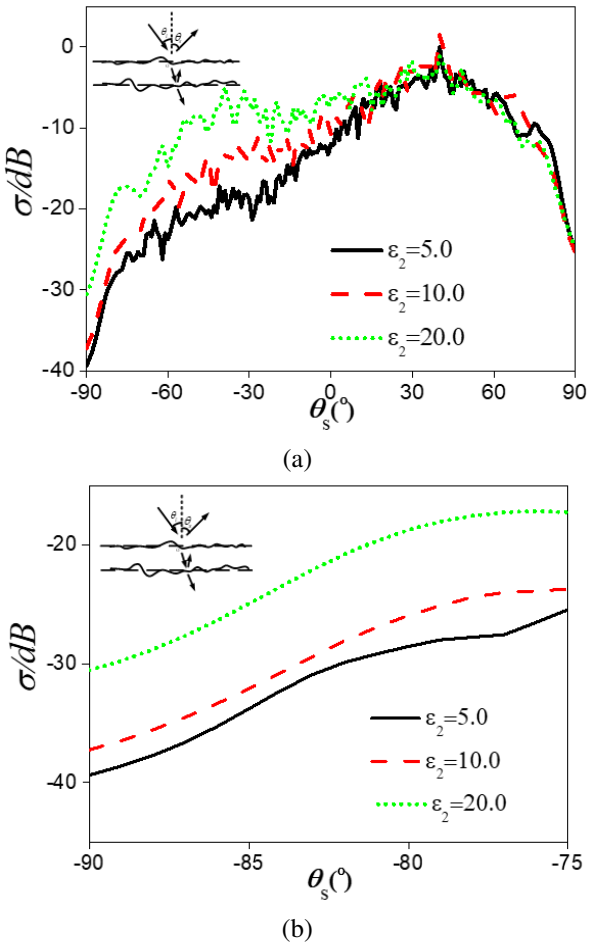

Fig. 9. Scattering coefficient comparison chart for different lower rough surface permittivity values: (a)-90°∼90° and (b) -90°∼75°.

V. CONCLUSION

This article proposes an innovative I-GFBM-SAA algorithm for effectively solving the electromagnetic scattering problem of rough surfaces. This algorithm significantly reduces the calculation workload from $o(N^3)$ to $o(N)$, thereby greatly saving computational time and improving computational efficiency. At the same time, this algorithm exhibits good convergence behavior under different calculation conditions, making it able to meet the computational needs of different application scenarios. The next research direction will be to incorporate targets (conductors and dielectrics) into the environment to further improve the electromagnetic scattering model and study composite electromagnetic scattering problems.

REFERENCES

[1] B. Wang, W. H. Wang, J. Fan, K. Q. Zhao, F. L. Zhou, and L. W. Tan, "Modeling of bistatic scattering from an underwater non-penetrable target using a Kirchhoff approximation method," *Defence Technology,* vol. 18, no. 7, pp. 1097-1106, 2022.

[2] P. Nicolas, B. L. Cedric, and B. Christophe, "Modeling of EM wave coherent scattering from a rough multilayered medium with the scalar Kirchhoff approximation for GPR applications," *IEEE Transactions on Geoscience and Remote Sensing,* vol. 58, no. 3, pp. 1654-1664, 2020.

[3] L. E. Richards, C. H. Song, and S. W. Hodgkiss, "Acoustic scattering comparison of Kirchhoff approximation to Rayleigh-Fourier method for sinusoidal surface waves at low grazing angles," *The Journal of the Acoustical Society of America,* vol. 144, no. 3, pp. 1269-1278, 2018.

[4] J. Tian, J. Tong, J. Shi, and L. Gui, "A new approximate fast method of computing the scattering from multilayer rough surfaces based on the Kirchhoff approximation," *Radio Science,* vol. 52, no. 2, pp. 186-195, 2017.

[5] W. Qing, L. Chen, Z. L. Ya, H. J. Qiang, and L. Lei, "High-order small perturbation method of arbitrary order for conducting rough surface scattering under TE incidence," *Applied Computational Electromagnetics Society (ACES) Journal,* vol. 35, no. 6, pp. 601-612, 2020.

[6] M. F. Arshad, A. Anwar, and M. A. Aqueel, "Perturbation method to study scattering from a dielectric-chiral rough interface," *Waves in Random and Complex Media,* vol. 31, no. 4, pp. 712-730, 2019.

[7] A. Saddek and D. Richard, "Scattering from 2-D perfect electromagnetic conductor rough surface: Analysis with the small perturbation method and the small-slope approximation," *IEEE Transactions on Antennas and Propagation,* vol. 66, no. 1, pp. 340-346, 2018.

[8] M. Sanamzadeh, L. Tsang, J. Johnson, R. Burkholder, and S. Tan, "Electromagnetic scattering from one dimensional random rough surfaces of dielectric layered media with waveguide modes using second order small perturbation method," *Progress In Electromagnetics Research B,* vol. 80, pp. 1-17, 2018.

[9] B. Auguié, W. R. C. Somerville, S. Roache, and E. C. L. Re, "Numerical investigation of the Rayleigh hypothesis for electromagnetic scattering by a particle," *Journal of Optics,* vol. 18, no. 7, 2016.

[10] C. Q. Shang, S. Z. Wu, T. Qu, and Z. J. Li, "Rayleigh model for electromagnetic scattering from a chiral sphere," *Procedia Engineering,* vol. 102, pp. 226-232, 2015.

[11] X. C. Li, X. Min, and D. D. Liu, "Rayleigh approximation for the scattering of small partially charged sand particles," *Journal of the Optical Society of America. A, Optics, Image Science, and Vision,* vol. 31, no. 7, pp. 1495-1501, 2014.

[12] K. C. Wang, Z. He, D. Z. Ding, and R. S. Chen, "Uncertainty scattering analysis of 3-D objects with varying shape based on method of moments," *IEEE Transactions on Antennas and Propagation,* vol. 67, no. 4, pp. 2835-2840, 2019.

[13] J. Chen, M. Zhu, M. Wang, S. Li, and X. Li, "A hybrid MoM-PO method combining ACA technique for electromagnetic scattering from target above a rough surface," *Applied Computational Electromagnetics Society (ACES) Journal,* vol. 29, no. 4, pp. 301-306, 2014.

[14] N. Basta and D. I. Olćan, "Scattering from anisotropic surfaces analyzed with method of moments," *Microwave and Optical Technology Letters,* vol. 60, no. 7, pp. 1782-1787, 2018.

[15] A. M. Mojtaba, S. S. H. Hesamedin, and D. A. Mojtaba, "A method of moments for analysis of electromagnetic scattering from inhomogeneous anisotropic bodies of revolution," *IEEE Transactions on Antennas and Propagation,* vol. 66, no. 6, pp. 2976-2986, 2018.

[16] S. Liu, B. Zou, and L. M. Zhang, "An FDTD-based method for difference scattering from a target above a randomly rough surface," *IEEE Transactions on Antennas and Propagation,* vol. 69, no. 4, pp. 2427-2432, 2021.

[17] H. Zamani, P. Dehkhoda, and A. Tavakoli, "Scattering by a three-dimensional buried object beneath multilayered rough surface illuminated by a collimated microwave Gaussian pulse," *AEUE - International Journal of Electronics and Communications,* vol. 123, 2020.

[18] R. C. Bollimuntha, F. M. Hadi, J. M. Piket-May, and A. Z. Elsherbeni, "Dispersion optimised plane wave sources for scattering analysis with integral based high order finite difference time domain methods," *IET Microwaves, Antennas & Propagation,* vol. 10, no. 9, pp. 976-982, 2016.

[19] J. Li, X. L. Guo, and H. Zeng, "FDTD investigation on electromagnetic scattering from two-dimensional layered rough surfaces," *Applied Computational Electromagnetics Society (ACES) Journal,* vol. 25, no. 5, pp. 450-457, 2010.

[20] D. Hrvoje, P. Dragan, and C. Mario, "On the edge element boundary element method/finite element method coupling for time harmonic electromagnetic scattering problems," *International Journal*

for Numerical Methods in Engineering, vol. 122, no. 14, pp. 3613-3652, 2021.

[21] J. J. Harman, C. Key, D. Estep, T. Butler, and B. M. Notaros, "Adjoint-based accelerated adaptive refinement in frequency domain 3-D finite element method scattering problems," *IEEE Transactions on Antennas and Propagation,* vol. 69, no. 2, pp. 940-949, 2021.

[22] X. Xu, C. Brekke, A. P. Doulgeris, and F. Melandsø, "Numerical analysis of microwave scattering from layered sea ice based on the finite element method," *Remote Sensing,* vol. 10, no. 9, p. 1332, 2018.

[23] Y. J. Wang, C. M. Tong, T. Wang, X. M. Li, and Q. K. Wang, "EM scattering of a target above canyon/valley environment based on composite rough surface modeling method and modified SBR-FBSSA algorithm," *Applied Sciences,* vol. 13, no. 7, p. 4427, 2023.

[24] Y. L. Du, J. J. Yin, X. Li, F. Gao, and J. Yang, "Accurate and efficient solution of electromagnetic scattering from randomly rough surface using MoM-SMCG with adaptive quadrature," *Electronics Letters,* vol. 57, no. 18, pp. 694-696, 2021.

[25] L. Li and J. Xu, "Electromagnetic scattering from perfectly conducting periodic rough surfaces using discrete two-level complex images method," *IOP Conference Series Materials Science and Engineering,* vol. 780, no. 5, 2020.

[26] A. Wang, J. Wang, Z. Huang, L. Guo, and T. Jian, "Fast simulations of electromagnetic scattering from one-dimensional rough surface over a frequency band using hybrid AMCBFM-Maehly method," *Journal of Engineering,* vol. 7, pp. 184622-184628, 2020.

[27] X. M. Li, J. J. Li, G. Qian, and P. C. Gao, "A hybrid method of solving near-zone composite electromagnetic scattering from targets and underlying rough surface," *Chinese Physics B,* vol. 29, no. 2, 2020.

[28] J. J. Wang, A. Q. Wang, T. Z. Jiang, and Z. X. Huang, "A fast algorithm for electromagnetic scattering from one-dimensional rough surface," *International Journal of Antennas and Propagation,* vol. 2019, no. 11, pp. 1-7, 2019.

[29] C. D. Moss, T. K. Grzegorczyk, H. C. Han, and A. K. Jin, "Forward-backward method with spectral acceleration for scattering from layered rough surfaces," *IEEE Trans Antennas Propagation,* vol. 54, no. 3, pp. 1006-1016, 2006.

[30] A. Iodice, "Forward-backward method for scattering from dielectric rough surfaces," *IEEE Trans. Antennas Propagation,* vol. 50, no. 7, pp. 901-911, 2002.

[31] D. Torrungrueng, H. T. Chou, and J. T. Johnson, "A novel acceleration algorithm for the computation of scattering from two-dimensional large-scale perfectly conducting random rough surfaces with the forward-backward method," *IEEE Trans. on Geoscience and Remote Sensing,* vol. 38, no. 4, pp. 1656-1668, 2000.

[32] H. T. Chou and J. T. Johnson, "A novel acceleration algorithm for the computation of scattering from rough surfaces with a forward-backward method," *Radio Science,* vol. 33, no. 5, pp. 1277-1287, 1998.

[33] A. Thorsos, "The validity of the Kirchhoff approximation for rough surface scattering using a Gaussian roughness spectrum," *Journal of the Acoustical Society of America,* vol. 83, no. 1, pp. 78-92, 1988.

Lilan Lei was born in Jiangxi, China. She received the bachelor's and master's degrees from Jiangxi Normal University, Jiangxi, China, in 2002 and 2009, respectively. Her research interests include computer applications and computer communication.